

Robust Time-Series InSAR Deformation Monitoring by Integrating Variational Mode Decomposition and Gated Recurrent Units

Peifeng Ma ¹, Senior Member, IEEE, Zeyu Jiao ², and Zherong Wu ³, Member, IEEE

Abstract—Continuous and large-scale surface deformation monitoring is critical for the comprehension of natural hazards and environmental changes. This can be facilitated by time-series interferometric synthetic aperture radar (TS-InSAR), which provides unprecedented spatial and temporal resolution. However, the original TS-InSAR measurements, being a superposition of trend, seasonal, and noise signals, often suffer from outlier and annual seasonal variations due to the influences of atmospheric delay, especially in coastal and mountainous areas, resulting in skewed monitoring if neglected. To address these issues, an integration method of variational mode decomposition and gated recurrent unit (VMD-GRU) is proposed in this study to enhance the robustness of continuous large-scale surface deformation monitoring. The VMD decomposes low-frequency trend, specific-frequency seasonal, and high-frequency noise components from the original TS-InSAR data via frequency-domain variational optimization first. Then, by eliminating the seasonal component decomposed by VMD from the original time series, the time series is reconstructed, effectively removing the influence of annual seasonal variations. Subsequently, GRU is utilized to further eradicate noise from the reconstructed time series, mitigating the influence of outliers and noise, thereby yielding a trend component that intuitively reflects surface deformation. Experiments on physical-based synthetic and real-world datasets demonstrate that the proposed VMD-GRU outperforms the existing methods. By introducing the frequency priors, the proposed method significantly enhances the robustness and accuracy of continuous large-scale surface deformation monitoring, providing a more reliable understanding of natural hazards and environmental changes.

Index Terms—Frequency priors, gated recurrent units (GRUs), surface deformation monitoring, time-series InSAR, variational mode decomposition (VMD).

I. INTRODUCTION

INTERFEROMETRIC synthetic aperture radar (InSAR) is a powerful geodetic technique enabling the remote

monitoring of Earth's surface under all conditions, with high resolution and wide spatial coverage. It has been proven fruitful in various geophysical applications such as earthquake, volcanic activity, and tectonic movement monitoring [1], [2], [3], [4], [5]. Time-series InSAR (TS-InSAR), an advanced iteration of the InSAR technique, harnesses time-series of SAR images or interferograms to precisely measure geodetic and geophysical parameters, including ground displacements [6], [7], [8]. The mitigation of atmospheric delays, a pivotal challenge in InSAR, is facilitated by TS-InSAR through temporal filtering and least-squares methods, thus enhancing the accuracy of deformation estimates [9], [10], [11]. The monitoring of surface deformation based on TS-InSAR is therefore of significant importance, providing high-precision, wide coverage, and consistent data for tracking earth movements.

When employing TS-InSAR for surface deformation monitoring, atmospheric delays in interferograms, resulting from changes in the refractivity of the atmosphere during two SAR acquisitions, are a significant source of error in TS-InSAR measurements [12], [13]. These delays comprise three main components: a short-scale component (few kilometers) likely introduced by turbulent or coherent dynamics in the troposphere [14]. A longer-scale component (tens of kilometers) potentially stems from lateral variations in pressure, temperature, or humidity. Finally, there is a topography-correlated component, which is due to changes in the pressure, temperature, or relative humidity as a function of height [15]. These atmospheric delays in TS-InSAR not only include systematic biases but also contain stochastic components, making these delays among the most challenging influencing factors to model accurately [16]. As a result, significant research efforts continue to explore the spatiotemporal characteristics of atmospheric delays to enhance the accuracy and reliability of TS-InSAR for surface deformation monitoring. The tropospheric delay, which can be divided into stratified and turbulent mixing delay, is due to the refraction of radar signals as they pass through the troposphere [14]. While the stratified delay is dependent on pressure and temperature and correlates with topography, the turbulent mixing delay primarily depends on water vapor variations, which are particularly severe in coastal and mountainous regions [17].

In the context of TS-InSAR, where the data consists of numerous images without extensive temporal gaps, the tropospheric delay can be assumed to be uncorrelated over time, as each image mainly captures the turbulent mixing delays [18], [19].

Manuscript received 2 April 2024; revised 5 June 2024; accepted 2 July 2024. Date of publication 11 July 2024; date of current version 15 January 2025. This work was supported in part by the National Natural Science Foundation of China under Grant 41971278, in part by Hong Kong Research Grants Council through General Research Fund under Grant 14223422 and Grant 14201923, and through the Areas of Excellence Scheme under Grant AoE/E-603/18, and in part by the CUHK Direct Grant for Research under Grant 4052294. (Corresponding author: Peifeng Ma.)

Peifeng Ma is with the Institute of Space and Earth Information Science, The Chinese University of Hong Kong Hong Kong, SAR, China, and also with the Shenzhen Research Institute, The Chinese University of Hong Kong, Shenzhen 518063, China (e-mail: mapeifeng@cuhk.edu.hk).

Zeyu Jiao and Zherong Wu are with the Institute of Space and Earth Information Science, The Chinese University of Hong Kong Hong Kong, SAR, China. Digital Object Identifier 10.1109/JSTARS.2024.3426676

For urban areas with low relief, the turbulent mixing delay often dominates the atmospheric delay, leading to the assumption that atmospheric noise in the InSAR deformation time series is stochastic. Common approaches to estimate and mitigate this atmospheric noise in the deformation time series involve low-pass temporal filtering techniques such as Gaussian and triangular filtering [20], [21]. However, the effectiveness of these methods greatly depends on parameter settings, like the choice of weighting strategies and the length of the filtering window. An inadequate filtering process could either leave residual noise in the deformation or obscure minor changes in the data.

As deep learning has made remarkable progress in fields such as computer vision [22], [23], speech recognition [24], and natural language processing [25], applying deep learning to TS-InSAR analysis shows considerable promise in alleviating atmospheric delay and improving monitoring accuracy. Recurrent neural network (RNN) and its variants, such as long short-term memory (LSTM) [26], and gated recurrent unit (GRU) [27], are specialized for discrete sequence analysis tasks such as time series denoising, forecasting, or change detection in the realm of remote sensing [28], [29]. Due to the nonstationary nature of InSAR data, previous studies usually divide its time series into three signals: seasonal, nonseasonal, and noise [30], [31]. This approach effectively improves the possibility of using deep learning to model different components in the InSAR time series.

Despite these advancements, two significant challenges remain when applying deep learning-based methods to continuous and large-scale surface deformation monitoring using InSAR data: 1) Annual seasonal variation. Existing deep learning methods assume seasonal components as static periodic functions irrespective of interannual variances in seasonal intensities, risking progressively cumulative monitoring errors [32]. 2) Abnormal outliers. Abnormal outliers in InSAR data, often stemming from atmospheric anomalies or instrumental errors, can significantly distort analysis, posing challenges to both traditional and deep learning models by potentially leading to overfitting and misleading interpretations of surface deformation trends [33].

For continued large-scale monitoring, ground deformation is related to geological conditions and is almost monotonous. Meanwhile, ground deformation exhibits seasonal variations mainly influenced by weather and hydrological conditions [34], [35]. Noise exists in every SAR image acquisition and is a component that changes at high frequency. This implies different frequencies associated with the three components of trend, season, and noise, which can be leveraged as prior information to improve the robustness of TS-InSAR analysis. To this end, this study proposes a robust surface deformation monitoring method integrating variational mode decomposition (VMD) and GRU. With VMD, frequency priors are introduced and the original TS-InSAR data is decomposed and reconstructed, which can eliminate the influence of annual seasonal variations. With GRU, the noise component is removed from the TS-InSAR and the influence of the outliers is mitigated, so that the trend component that can intuitively reflect the surface deformation state is extracted. The integration of VMD with GRU, by introducing frequency priors of TS-InSAR, can not only effectively enhance

the model's robustness to annual seasonal variations, but can also mitigate the influence of outliers, which is critically important for improving the robustness and accuracy of continuous and large-scale surface deformation monitoring.

The rest of this article is organized as follows. Section II presents the method for obtaining TS-InSAR, and presents and introduces the architecture of the proposed VMD-GRU model. Section III conducts experiments on synthetic and real-world data to verify the robustness and effectiveness of the proposed VMD-GRU method. Section IV discusses the robustness of the proposed model to annual seasonal variation, the effect of time series reconstruction on the model performance, the generalization of the proposed method to different revisit periods, and the limitations of this study. Finally, Section V draws conclusions and directions for future work.

II. METHODOLOGY

This study proposes a novel perspective on TS-InSAR data through the lens of the frequency domain. The crucial aspect of pre-existing knowledge pertaining to the frequency of each data component has often been disregarded when identifying their causes. As previously stated, surface deformation trends are predominantly influenced by geological and hydrological conditions, resulting in largely monotonic variations over continuous monitoring. This implies that the trend component corresponds to a low-frequency signal. The seasonal component, cycling annually, aligns with a specific frequency signal. While the noise component, inherent in every acquisition, corresponds to a high-frequency signal in each sample. Therefore, when viewed from the frequency domain, each TS-InSAR component should manifest distinct boundaries on the frequency domain. To this end, this study implements VMD to segregate each component within the frequency domain, decomposing trend, seasonality, and noise components into separate frequency bands.

This section outlines the acquisition process of time series data on surface deformation using robust multitemporal InSAR. Subsequently, the proposed VMD-GRU model is detailed, outlining its potential to improve the robustness of TS-InSAR-based deformation monitoring. The overall workflow of the proposed method is depicted in Fig. 1.

A. Robust Multitemporal InSAR for Acquiring Time Series Data

This study employed a robust two-tier multitemporal InSAR method [36] for the detection of Persistent scatterer (PS) and distributed scatterer (DS) points to acquire time series data for surface deformation monitoring, as demonstrated in Fig. 1. The coregistration of SAR images was achieved through a purely geometric algorithm, facilitated by SRTM DEM data [37]. This was subsequently followed by differential interferometry with a multilook of 8×2 . The design of a two-tier network was introduced for the identification of PS and DS, without the necessity for preliminary atmospheric removal across the whole area. PS candidates were handpicked with an amplitude dispersion value of 0.3, and subsequently linked within a densified Delaunay network. Following the phase differentiation of two connected

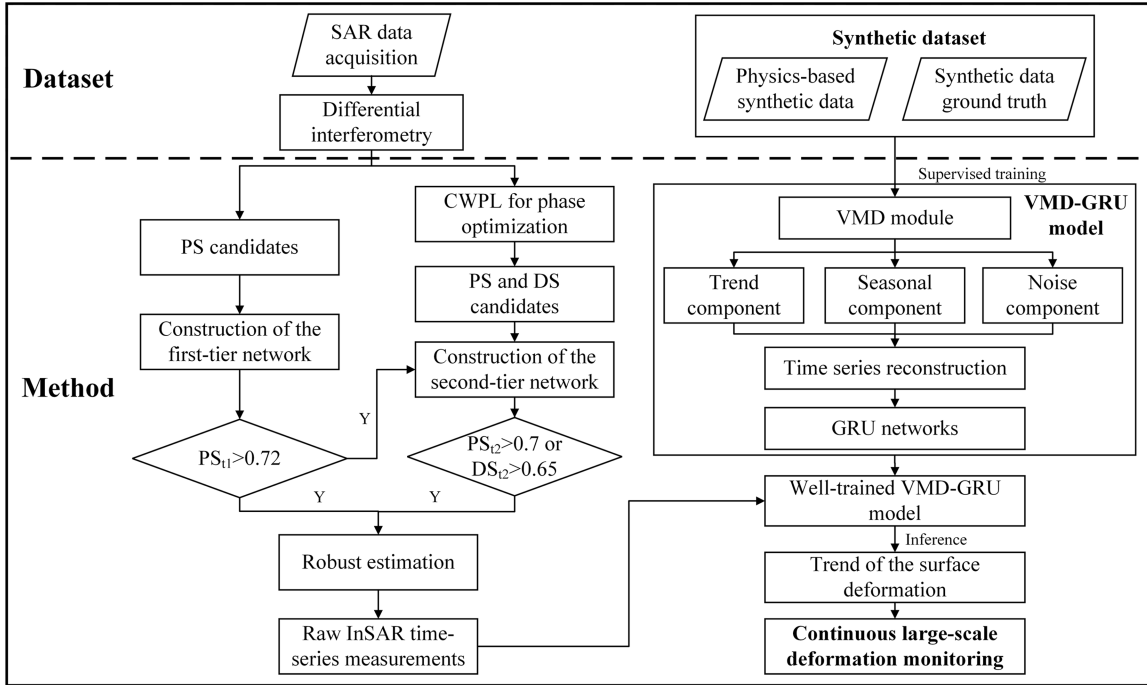


Fig. 1. Workflow of the proposed robust surface deformation monitoring method.

PS candidates, the signal model could be expressed as

$$y = A\Upsilon \quad (1)$$

where $y = [y_1, \dots, y_{N_s}]^T$ (N_s is the number of SAR images) represents the differential interferograms, Υ stands for a $N_s \times 1$ vector that includes the complex reflectivity of all objects equidistant to the SAR sensor, and A denotes the sensing matrix containing $a(\Delta h, \Delta v)$ within its columns (Δh and Δv) represent the sampled relative height and deformation velocity between two PS candidates, respectively.

The combined utilization of beamforming and a robust M-estimator facilitated the inversion of (1) and the estimation of Υ . Should the maximum element in $\text{abs}(\Upsilon)$ exceed the preset threshold of $PS_{t1} = 0.72$, the arc was preserved, and the corresponding height and deformation velocity could be extracted. The temporal coherence PS_{t1} of the first-tier network was set to 0.72 based on practical experience. For C-band Sentinel-1 interferometric measurements, temporal coherence thresholds of $|\hat{\gamma}| = 0.72, 0.8, 0.9, 0.95, \text{ and } 0.975$ correspond to estimated $\hat{\sigma}_{\text{disp}}$ values of 3.6, 3, 2, 1.44, and 1 mm, respectively [58]. The 1 mm threshold represents an indicative limit on the accuracy of C-band deformation measurements. Setting the temporal coherence threshold to 0.72 ensures that the precision of deformation measurements is better than 3.6 mm, meeting the precision requirements for measuring mining-induced subsidence. Relative parameters were then integrated via network adjustment, which included the implementation of a ridge estimator to counteract potential ill-conditioning in the robust parameter integration.

The most stable PSs were extracted from the densified Delaunay network, serving as a reference for the detection of further PS and DS points. The adoption of an omnidirectional point extension strategy allowed for the progressive construction of

local networks and multidirectional extension. For DS detection, SqueeSAR optimizes the differential phase through the application of the Broyden–Fletcher–Goldfarb–Shanno algorithm, which necessitates the inversion of covariance matrix C [38]. However, the inversion process may yield unreliable results if C is not positive definite, potentially introducing further errors. To rectify this issue, the optimal phase was calculated using coherence-weighted phase-linking (CWPL). Temporal coherence thresholds for identifying additional PSs and DSs were established at $PS_{t2} = 0.7$ and $DS_{t2} = 0.65$, respectively.

The line of sight (LOS) deformation velocity and time-series deformation of all PS and DS points were ultimately ascertained. For vertical surface deformation monitoring, the surface LOS deformation can be divided by $\cos(\theta)$ (where θ is the incident angle) and converted into vertical deformation. In steep terrains, LOS deformation can be converted to the downward direction, using the slope gradient under the assumption that slope movements correspond to the downward direction.

B. TS-InSAR Decomposition Based on VMD

VMD is an unsupervised signal decomposition method that excels in analyzing complex nonstationarity signals into a set of nearly orthogonal intrinsic modes. Through alternating minimization of the sum of the estimated spectral bandwidths, VMD effectively decomposes a signal by seeking the analytic signals of various modes with minimal bandwidths [39]. In contrast to traditional methods such as empirical mode decomposition [40] and wavelet transform [41], VMD offers superior nondistortion, analytical solutions, and fewer parameters. Coupled with its capacity to deliver compact mode information and to analyze the inherent structures of complex datasets, VMD has found

extensive use in image processing, biomedical signal analysis, and a variety of other fields [42], [43].

VMD operates based on the premise that a signal is a superposition of subsignals or intrinsic mode functions (IMFs), each dominated by distinct frequencies. To qualify as an IMF, a function must meet two criteria: 1) The number of local extremum points and zero-crossing points across the entire function's time range must be either equal or differ by no more than one. 2) At any time point, the mean value of the envelope of the local maximum (upper envelope) and the envelope of the local minimum (lower envelope) must be zero. This assumption aligns with the decomposition of TS-InSAR into three distinct frequency components.

IMFs are defined as amplitude-modulated-frequency-modulated signals [44], expressible as

$$s_k(t) = a_k(t) \cos(\phi_k(t)) \quad (2)$$

where the phase $\phi_k(t)$ is nondecreasing, and the signal envelope $a_k(t)$ is non-negative. Furthermore, $s_k(t)$ is assumed to be a real signal, hence its analytical signal is

$$s(t) = s_k(t) + jH[s_k(t)] \quad (3)$$

where H is the Hilbert transform [45], and its system transfer function is $\hat{h}(w) = -j \operatorname{sgn}(w)$.

Under the premise of VMD, all components are deemed narrow-band signals concentrated around their individual center frequencies. Thus, VMD establishes a constrained optimization problem based on the narrowband condition of the component, facilitating the estimation of the signal component's center frequency and the corresponding component's reconstruction. This optimization problem can be represented mathematically as

$$\begin{aligned} \min_{\{u_k\}, \{\omega_k\}} & \left\{ \sum_k \left\| \partial_t [(\delta(t) + j\pi t) * u_k(t)] e^{-j\omega_k t} \right\|_2^2 \right\} \\ \text{s.t.} & \sum_k u_k(t) = f \end{aligned} \quad (4)$$

where f denotes the input signal, u_k represents the k th component decomposed from signal f , ω_k denotes the centre frequency of component u_k , $\delta(t)$ is the Dirac delta function, $*$ denotes convolution operation, $\frac{\partial}{\partial t}[\cdot]$ calculates the differential of $[\cdot]$ with respect to time t , $\|\cdot\|_2$ computes the 2-norm of $[\cdot]$.

The optimization problem seeks to minimize the sum of Hilbert transform smoothness of all components $\left\| \frac{\partial}{\partial t} [(\delta(t) + j\pi t) * u_k(t)] e^{-j\omega_k t} \right\|_2^2$ under the constraint that the sum of components is equal to the original signal f ($\sum_k u_k(t) = f$). To solve this problem, the above-equality-constrained optimisation problem can be transformed into an unconstrained optimization problem through an augmented Lagrangian [46], [47], expressed as

$$\begin{aligned} & L(\{u_k\}, \{\omega_k\}, \lambda) \\ := & \alpha \sum_k \left\| \partial_t \left[\left(\delta(t) + \frac{j}{\pi t} \right) * u_k(t) \right] e^{-j\omega_k t} \right\|_2^2 \end{aligned}$$

$$+ \left\| f(t) - \sum_k u_k(t) \right\|_2^2 + \left\langle \lambda(t), f(t) - \sum_k u_k(t) \right\rangle. \quad (5)$$

The solution to this constrained problem can be obtained via the alternate direction method of multipliers [48], [49], [50], which proposes updating one of the variables while keeping the other two variables fixed, as represented in the following equations:

$$u_k^{n+1} = \operatorname{argmin}_{u_k} L(\{u_{i < k}^{n+1}\}, \{\omega_k^n\}, \lambda^n);$$

$$\omega_k^{n+1} = \operatorname{argmin}_{\omega_k} L(\{u_k^n\}, \{\omega_{i < k}^{n+1}\}, \lambda^n);$$

$$\lambda^{n+1} = \lambda^n + \rho \left(f(t) - \sum_k u_k^{n+1}(t) \right). \quad (6)$$

VMD, bolstered by a solid mathematical framework, essentially operates as an adaptive optimal Wiener wave filter group. The specification of its target IMF number significantly impacts its decomposition accuracy [43], [51]. For TS-InSAR data, the frequency difference of the three components of trend, season, and noise is introduced into the model as prior knowledge, setting the corresponding number of target IMFs to three. This ensures that the decomposition of TS-InSAR data is underpinned by a clear physical basis. Further details on VMD's implementation can be found in Appendix A.

C. Integrated VMD-GRU Model

The integration of VMD and GRU methods, as depicted in Fig. 1, forms a potent method for the monitoring of large-scale surface deformation, boasting increased robustness and precision. This section delves into the rationale behind this integration and provides insights into the effective merger of the two methods. The chief purpose behind amalgamating VMD with GRU is the augmentation of the robust qualities of both time series data processing methods, as well as offsetting their respective limitations. Among them, VMD facilitates the decomposition of TS-InSAR data into multiple frequency signals, enabling the identification of various deformative components in the data. However, VMD's effectiveness may be compromised by high noise and mode mixing in the decomposition results due to its unsupervised nature. Such limitations can result in decreased decomposition accuracy and misinterpretation of similar frequency components.

This section delves into the rationale behind this fusion and provides insights into the effective merger of the two methodologies. The chief purpose behind amalgamating VMD with GRU is the augmentation of the robust qualities of both time series data processing methods, as well as offsetting their respective limitations. The usage of VMD leads to the fragmentation of TS-InSAR data into a range of frequency components, thus paving the way for the identification of unique deformation signals in the data. Despite its strengths, VMD, an unsupervised mode decomposition method, is vulnerable to noise interference and mode mixing (such as low-frequency outliers) in the results of the decomposition. In high-noise environments, the accuracy

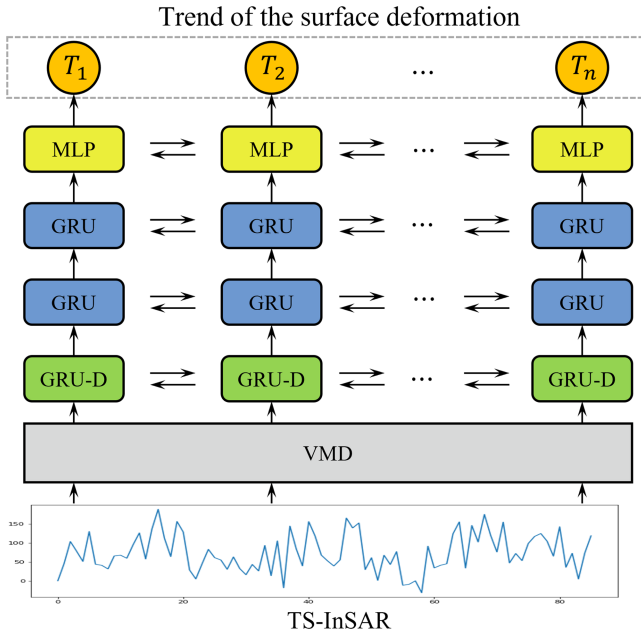


Fig. 2. Architecture of the proposed VMD-GRU model.

of the decomposition outcomes diminishes, leading to the potential fusion of similar but distinct frequency components into one mode, or the fragmentation of a single mode into various components. This limitation could cause the failure of VMD in accurately capturing complicated, nonlinear deformation patterns, particularly in prolonged monitoring scenarios. However, VMD offers the significant benefit of removing annual seasonal variances in regions experiencing significant atmospheric delay, as it uses the prior knowledge of specific seasonal signal frequency. On the other hand, GRU, a specialized type of RNN, has demonstrated remarkable success in predicting time-series data with nonlinear patterns [27]. Although GRU performance is limited in nonstationarity time series, it can model the temporal dependency of a single component over a long period, making it ideal for continuous and large-scale monitoring of surface deformation. Thus, integrating VMD and GRU can result in a hybrid model with superior performance. The proposed VMD-GRU model architecture is illustrated in Fig. 2.

In this study, inspired by [52], a layer of GRU with decay (GRU-D) is utilized to address the issue of potential missing values in TS-InSAR data. Subsequently, two layers of GRU further extract the features of the reconstructed time series, mapping the extracted features into separated trend components through multi-layer perception (MLP). The implementation details of GRU and GRU-D are presented in Appendix B. To better utilize the contextual content of time series data for noise removal, all networks in the model are set to bidirectional connectivity [53].

As depicted in Fig. 2, the VMD-GRU model operates on two primary levels: reconstruction and decomposition. Initially, TS-InSAR data is decomposed into several IMFs via VMD, each IMF representing a distinct frequency band of the component. This can be mathematically represented as

$$F(t) = \sum_{k=1}^K \text{IMF}_k(t) + R_t \quad (7)$$

where $F(t)$ represents the original TS-InSAR data, $\text{IMF}_k(t)$ denotes the k th IMF and K signifies the total number of IMFs. R_t stands for the residual noise value postdecomposition. This value is typically minimal and is determined by the parameter τ in VMD, which is used to ascertain the convergence of VMD after numerous iterations. Based on the aforementioned decomposition outcomes, the IMF corresponding to the seasonal component IMF_s is subtracted from the original time series, thus leading to the reconstruction of the original signal. Why this method of reconstructing first and then decomposing will be elaborated in the discussion section later. This computation can be represented as

$$\text{Rec}_{ts} = F(t) - \text{IMF}_s. \quad (8)$$

In the decomposition stage, the reconstructed signal is fed into the stacked GRU networks for the extraction of trend components. Owing to the ability of GRU-D and GRU to handle complex temporal dependencies, the trend component can be extracted from the reconstructed signal. The effective combination of these methods exploits the feature extraction capability of VMD and the powerful temporal modeling capabilities of GRU, culminating in superior prediction performance. Furthermore, this model benefits from the application of separate GRU networks on each IMF, which aids in capturing distinct temporal patterns existing in different frequency bands. Consequently, the VMD-GRU model allows for more robust and precise monitoring of continuous and large-scale surface deformation.

III. EXPERIMENTS AND RESULTS

In this section, the efficacy of the proposed VMD-GRU is elucidated through the analysis of synthetic data and real-world data from the Lantau Island and the Guangdong-Hong Kong-Macao Greater Bay Area (GBA). The performance of the VMD-GRU model is juxtaposed against commonly used Gaussian filters and the original GRU model.

A. Experimental Data

The data used in the performance evaluation encompasses both synthetic and real-world data. Synthetic data, designed in line with [32] (termed as GRU model in the following), are produced based on physical mechanism simulations tailored to the requirements of the deep learning model. Synthetic data consists of the amalgamation of three components: trend, season, and noise. Thus, synthetic data $X(t)$ can be formulated as follows:

$$X(t) = (\text{Trend}(t) + \text{Season}(t) + \text{Noise}(t)) \cdot M(t) \quad (9)$$

where $\text{Trend}(t)$ represents the trend component, which may display linear, decelerating, or accelerating behavior as outlined by [31]. The seasonal component is represented as $\text{Season}(t)$. $\text{Noise}(t)$ signifies the noise component. A binary mask matrix, $M(t)$, indicates the possible missing values within the time series, a frequent occurrence in TS-InSAR data. GRU-D model aids in managing these missing values, thus reducing their impact on the accuracy of deformation monitoring results.

Synthetic datasets are fabricated as the reverse process of InSAR data acquisition according to physical mechanisms.

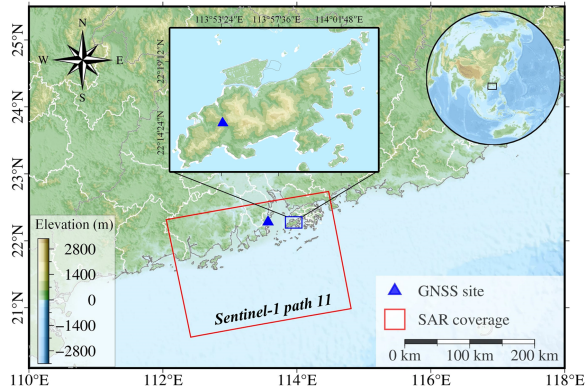


Fig. 3. Location of the real-world study area. The red box is the SAR coverage area, and the blue triangle indicates the positions of the GNSS stations.

Therefore, individual components and their ground truth values are annotated, thereby providing a quantitative metric for the performance evaluation of the proposed VMD-GRU against other existing methods. In addition to the synthetic data, real-world InSAR data forms an integral part of the experimental datasets. To comprehensively assess the robustness of the proposed VMD-GRU, Lantau Island (coastal areas with strong terrain) near Hong Kong airport and the GBA were selected as the study area, as shown in Fig. 3. These regions, located in the subtropical region of southern China, experience frequent cloudy and rainy weather, leading to the amplification of atmospheric noises in InSAR signals. Lantau Island was chosen to demonstrate the effectiveness of the proposed method in coastal areas with strong terrain variations. Proximate to the Hong Kong Airport, whose Ts-InSAR data were used to validate the GRU model, Lantau Island exhibits significant topographical variations compared to the relatively flat Hong Kong airport, thereby contributing to stratified delays in TS-InSAR that cannot be ignored. Surface deformation monitoring data from a GNSS station on Lantau Island was obtained to validate the proposed method's effectiveness in monitoring surface deformation trends. In addition, to further verify the proposed method's robustness on a larger spatial scale, data from the GBA, covering several cities and a GNSS station in Zhuhai city, was used.

Sentinel-1 SAR images for these areas, spanning from January 1, 2019, to December 27, 2021, were processed using the robust multi-temporal InSAR method to procure the time-series data of the measurement points within these regions. Ideally, satellites Sentinel-1A and Sentinel-1B collect SAR images at 12-day intervals, and their combined use allows for observations at 6-day intervals. In this study, a total of 88 SAR images were obtained at a minimum interval of 12 days due to the low sampling rate over Hong Kong. Accordingly, over the period from 1 January 2019 to 27 December 2021 with a 12-day interval, the number of SAR images should be 92. However, with 4 (92-88) missing observations, the missing rate approximates 4.3%.

B. Model Configuration and Training

The experiment configuration and execution utilize a Windows operating system, Python programming language, and the TensorFlow deep learning framework [54]. All experimentations

were conducted on a GeForce GTX 3090 GPU, with 24 GB RAM and an Intel i7-11700KF CPU with 64 GB RAM. The training process for the VMD-GRU model is performed on a dataset composed of 60 000 synthetic time series in accordance with the synthetic dataset specifications of the construction of the original GRU model. The dataset includes 20 000 samples for each of decelerating, accelerating, and linear deformation trend types, inclusive of stable deformations. In the VMD-GRU model, both the GRU-D and GRU layers consist of 64 hidden units. A dropout rate of 0.2 is imposed on the GRU layers and the subsequent MLP to improve model generalization and prevent overfitting. The model parameters are optimized using the Adam method [55], [56], with the aim of minimizing the mean squared error (MSE) loss. Early stopping is employed to identify the best weights for the model, with the validation dataset comprising 9000 synthetic time series. All input time series are globally normalized within a range of -1 to 1 for consistency, while output supervisions retain their original values. The initial learning rate is set at 3×10^{-4} and the batch size for training and testing is fixed at 64.

C. Evaluation of Synthetic Data

Since synthetic data is embedded with ground truth, it is an ideal tool for the quantitative evaluation of the proposed VMD-GRU method. Utilizing the same configuration as the GRU model, this study generates 20 000 diverse synthetic time series to test the proposed VMD-GRU model and compare it with other existing methods, including temporal Gaussian filtering with various standard deviation σ parameters and the GRU model. Temporal Gaussian filtering is a frequent choice for InSAR time series denoising, although it necessitates careful selection of the appropriate standard deviation σ parameter. The σ value is tested at 1, 2, 3, and 4 to empirically ascertain the optimal parameter choice for temporal Gaussian filtering. For missing values, Gaussian filtering discards missing time steps, utilizing only available data within the filtering window for output. The GRU model directly employs the original TS-InSAR data as input. Its key divergence from this study lies in its lack of VMD usage to introduce frequency priors for data reconstruction. Notably, separating deformation trends from raw TS-InSAR data is a sequence-to-sequence multioutput regression task, where output values are not independent. Several machine learning algorithms inherently support this type of multiple-output regression, with decision trees being a popular example. Despite this, decision trees for multiple output regression may encounter limitations, as the relationship between inputs and outputs can become blocky or highly structured based on the training data. Furthermore, the performance is sensitive to tree depth. If the tree's maximum depth is set too high, it may overlearn the fine details of the training data and consequently overfit the noise. More importantly, traditional machine learning methods often struggle with optimization due to the interdependence of hundreds of output values, and thus were not selected as baselines for comparative experiments.

The quantitative results from the experiments on synthetic datasets are presented in Table I. The proposed VMD-GRU model exhibits comparable performance to the original GRU

TABLE I
EVALUATION RESULTS ON THE SYNTHETIC TESTING DATASET

Metric	Gauss				GRU	VMD-GRU
	$\sigma=1$	$\sigma=2$	$\sigma=3$	$\sigma=4$		
MSE	8.842	5.053	5.442	8.518	3.528	3.287
MAE	2.352	1.781	1.850	2.311	1.485	1.522

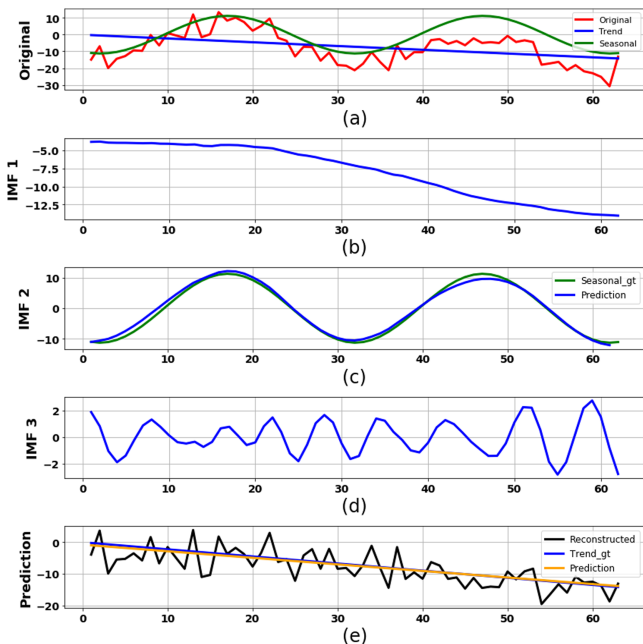


Fig. 4. Example of the proposed VMD-GRU on synthetic data. (a) Is the original synthetic data, where the red is the synthetic time series data, and the ground truth trend and seasonal signals are represented in blue and green, respectively. (b)–(d) Three components separated by VMD, corresponding to trend, season and noise respectively. The green line in (c) represents the ground truth of the seasonal component, consistent with the green in (a). The black in (e) represents the reconstructed time series after removing the seasonal component separated by VMD, and the blue is the ground truth trend component, which is consistent with that in (a). The trend component separated after VMD-GRU is indicated in orange.

model and significantly outpace temporal Gauss filtering methods, which are heavily dependent on appropriate parameter choice. In addition, when σ is 2, the Gaussian filter achieves the best performance, so when visualizing the trend estimation results, only σ equal to 2 is displayed.

In addition, a visual representation of the synthetic time series data processing using VMD-GRU is provided in Fig. 4, demonstrating the original signal reconstruction process and deformation trend extraction. Fig. 4 shows promising aptitude in extracting seasonal components. The deformation trend derived from the reconstructed signal aligns closely with the ground truth.

In addition, the proposed VMD-GRU is also evaluated under different trend types. As depicted in Fig. 5, the proposed method

shows good performance under different trends. It merits mention that the synthetic data is generated following a physical mechanism assumption, in which there is no large change in the amplitude of the seasonal signal, and the annual seasonal variation is not fully considered. As such, the synthetic data can be viewed as a unique subset of real-world data where differences in annual-seasonal components are absent. The performance similarity of the VMD-GRU to the GRU model in such circumstances demonstrates the feasibility of the VMD-GRU model for continuous surface deformation monitoring based on TS-InSAR. The presence and impact of variations between annual seasons will be further explored through experiments detailed in the subsequent sections.

D. Evaluation of Real-World Data

Unlike synthetic data, where the annotated ground truth can be leveraged as a reference, most of the real-world data are not manually annotated, but the spatial distribution of deformation can be qualitatively analyzed or validated using nearby GNSS stations or existing research. This section contains two areas, the validation on Lantau Island and the performance on GBA.

1) *Validation on the Lantau Island:* The Lantau Island, proximate to Hong Kong airport where the original GRU model was validated, has been selected as one of the study areas. This area is characterized by strong terrain in contrast to the airport's low terrain. The study area is depicted in Fig. 3, which also contains a GNSS station (represented by a blue triangle in Fig. 3). The surface deformation data gathered by this station, collected by the Nevada Geodetic Laboratory of the University of Nevada, Reno, are available for public access [57] and serve as an empirical benchmark to validate the performance of different methods.

In an endeavor to validate the proposed VMD-GRU method's robustness in strong terrain areas, Sentinel-1 SAR data of Lantau Island are processed using the Gauss filtering, the original GRU model, and the proposed VMD-GRU. The spatial distribution of cumulative deformation over different periods is showcased in Fig. 6.

As revealed in Fig. 6(a) and (c), the original GRU model fails to yield effective results in regions with strong terrain. Unremoved seasonal variations accumulate in the trend component, manifesting an overall upward surface deformation trend. Contrarily, the trend component extracted by the proposed VMD-GRU demonstrates commendable resilience to terrain changes. Temporal Gaussian filtering removes some noise interference but may also cause some trend components to be removed unnecessarily. In addition, it can be clearly seen in Fig. 6(c) that temporal Gaussian filtering cannot deal with the impact of strong terrain. As the altitude increases from west to east, the surface deformation appears an undue overall uplift. Fig. 6(b) shows an obvious outlier in TS-InSAR. The original signal suddenly dropped below 0. Although both temporal Gaussian filtering and the original GRU model have corrected this outlier to a certain extent, it can be seen that the deformation value increases with the elevation from west to east, obviously there have been regional changes that should not have occurred. The original

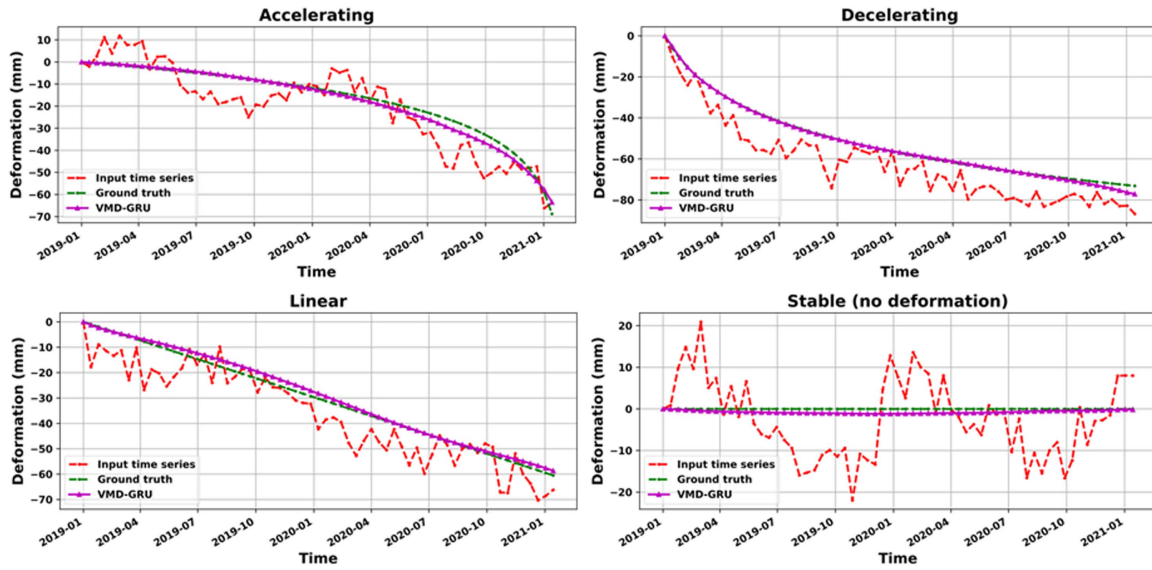


Fig. 5. Evaluation of the VMD-GRU model performance under different trend types.

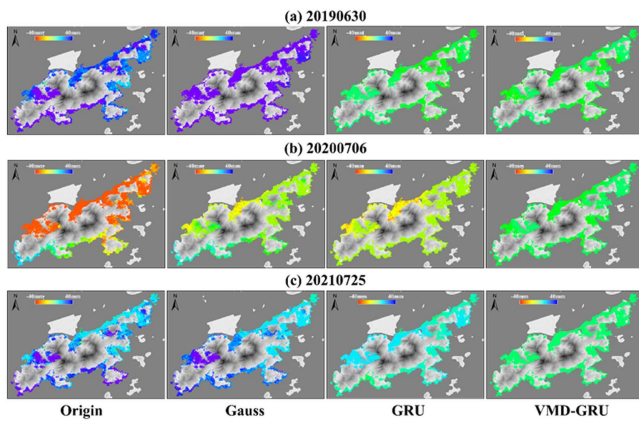


Fig. 6. Spatial distribution of cumulative deformation in different periods.

GRU model is affected by outliers, and the overall values are not robust. This highlights the challenges faced by the original GRU model in effectively managing outliers with contextual content of time series. Conversely, the proposed VMD-GRU method displays strong robustness to outliers. It preprocesses outliers in the time domain while reconstructing the signal, thereby ensuring the accuracy of continuous monitoring.

To further evaluate the effectiveness of the proposed method in the time domain, the data of a measurement point located near the GNSS station is extracted as an input. Fig. 7 illustrates the results of different methods on the time series data obtained from Lantau Island, including the original GRU model, VMD-GRU, and GNSS station’s measurements, respectively. Among them, the deformation measured by the GNSS station is strictly quality-controlled by Nevada Geodetic Laboratory solutions and thus can be considered a true deformation of the Earth’s surface [57]. But this measure also incorporates seasonal variation, so the average deformation rate can be considered to closely reflect the deformation trend.

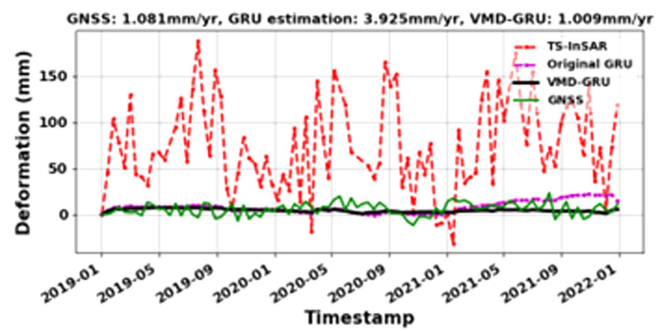


Fig. 7. Results of different methods on the time series data obtained from Lantau Island. The red line is the original InSAR time series, the wine-red line is the surface deformation trend estimated by the original GRU model, the black line is the proposed VMD-GRU estimated surface deformation trend, and the green line is the GNSS measurement. The annual average deformation velocity obtained by GNSS, the original GRU model, and the VMD-GRU are 1.081, 3.925, and 1.009 mm/yr, respectively.

Observing the results presented in Fig. 7, annual seasonal variations are discernible in the original time series data across three years from 2019 to 2021. The original GRU model fails to separate the trend component from the seasonal component fully when extracting the trend component. Consequently, residual seasonal signals accumulate in the trend component, leading to an overall V-shaped trend component. Also as shown in Fig. 7, the annual average deformation velocity estimated by GNSS is 1.081 mm/yr, original GRU model is 3.925 mm/yr, and VMD-GRU is 1.009 mm/yr. VMD-GRU has achieved a level far exceeding the original GRU model and is closer to the estimated value of GNSS.

Further, the VMD’s decomposition results for the time series data mentioned above are depicted in Fig. 8. Fig. 8(a) illustrates the original time series, the seasonal components decomposed by VMD, and the reconstructed time series from top to bottom. Fig. 8(b) exhibits the spectrum diagram during the decomposition process of each component, signifying the convergence

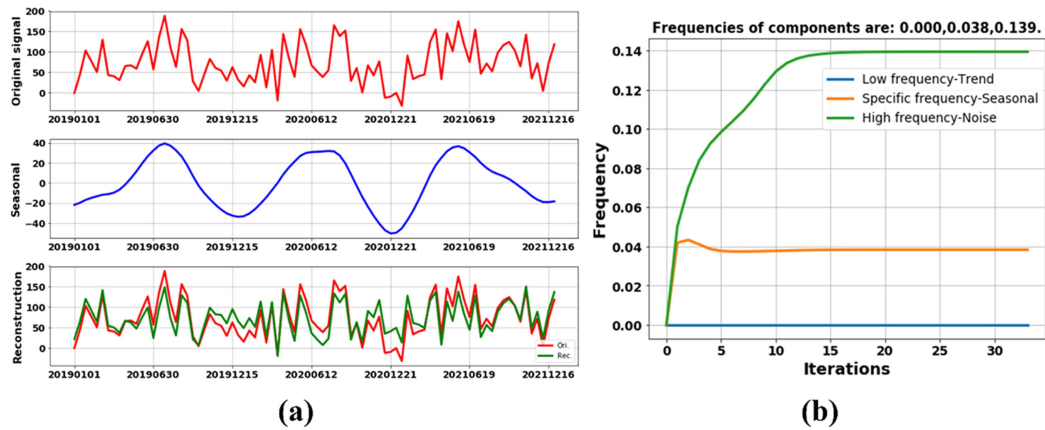


Fig. 8. Decomposition results of VMD for the above time series data. (a) Is the original time series, the seasonal components decomposed by VMD, and the reconstructed time series from top to bottom. (b) Is the spectrum diagram during the decomposition process of each component.

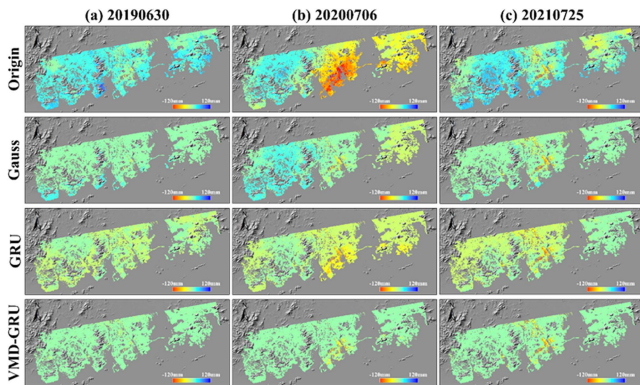


Fig. 9. Test results of different methods on GBA data. Each row corresponds to the cumulative deformation spatial distribution of the surface in different periods, and each column corresponds to the original time series data, results of the Gaussian filtering, results of the original GRU model, and results of the VMD-GRU.

process of the VMD decomposition signal from the perspective of the frequency domain. When it finally converges, the frequency of the corresponding seasonal signal is approximately 0.038, and its corresponding period is about 26, which is highly consistent with the acquired TS-InSAR data period. Given Sentinel-1's revisit period of 12 days, the theoretical year encompasses about 30 timestamps. This corresponds to a frequency of about 0.033, with an error of about 6.1% $[(0.033-0.035)/0.033]$ relative to the seasonal frequency of VMD decomposition. This may be due to the existence of missing values, and small differences between the frequency of the seasonal component of the VMD decomposition and the true frequency.

2) *Performance on GBA Data*: After demonstrating the effectiveness of the proposed VMD-GRU method in areas with strong terrain, further validation is performed in the context of the GBA, to confirm the model's robustness in large-scale surface deformation monitoring. The study area in GBA is marked by a red box in Fig. 3, and the performance of the various methods on GBA data is presented in Fig. 9.

The substantial spatial inhomogeneity is presented in the original data (topmost row of Fig. 9) of the large-scale GBA. The

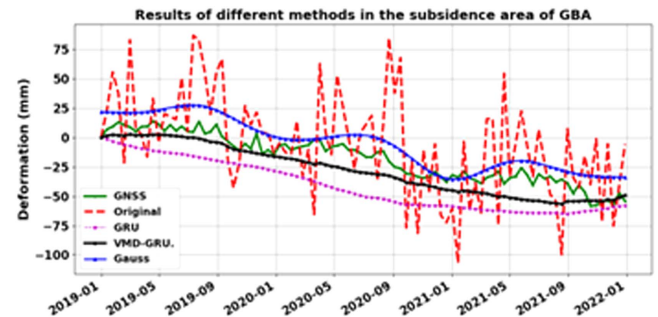


Fig. 10. Test results of different methods in the subsidence area of GBA.

temporal Gaussian filtering significantly suppresses the noise signal, yet it also runs the risk of unnecessarily removing portions of the deformation signal. In addition, temporal Gaussian filtering can only eliminate noise that obeys random distribution from the time series, and it is effective for the noise effect caused by strong terrain, and there is still a large amount of noise remaining in the mountainous area of the GBA.

The implementation of the original GRU model presents a substantial improvement in spatial inhomogeneity, even though large, interconnected deformation regions endure. Even certain areas in Hong Kong previously exhibiting minor deformation are misinterpreted as uplift by the original GRU model. In terms of spatial distribution, the original GRU model's impact resembles the effect of temporal Gaussian filtering with a standard deviation (σ) of 2, corroborating the findings of prior research [32]. Following the VMD-GRU, the surface deformation trend remains largely unaffected by topography. In addition, relevant settlements, such as those in Zhuhai [Fig. 9(b), red area of the origin], which align with prior studies [13], are well preserved within the VMD-GRU results. This emphasizes the utility of VMD-GRU in preserving important deformation information while effectively managing spatial inhomogeneities and noise effects. Fig. 10 presents the results of different methods in the subsidence area of GBA. It can be seen from the results that the estimation obtained by VMD-GRU are closer to the data obtained by GNSS stations than the temporal Gaussian filtering and the original GRU model.

TABLE II
EVALUATION RESULTS ON THE SYNTHETIC TESTING DATASET WITH ANNUAL SEASONALITY CHANGE

Metric	Gauss				GRU	VMD-GRU
	$\sigma=1$	$\sigma=2$	$\sigma=3$	$\sigma=4$		
MSE	11.329	8.662	8.102	8.340	6.528	3.937
MAE	5.667	6.131	3.063	4.283	4.875	2.010

The empirical experiments conducted on synthetic data, Lantau Island data, and GBA data demonstrate that the proposed VMD-GRU exhibits formidable robustness against time-series signals superimposed by multiple components, noise, and strong terrain. This robustness is immensely valuable for the continuous and large-scale monitoring of surface deformation.

IV. DISCUSSION

A. Robustness to Annual Seasonal Variation

Fig. 7 reveals the widespread presence of annual differences in TS-InSAR through a comparison of TS-InSAR time series data and GNSS station measurement data. To assess the impact of annual seasonal differences, the synthetic data method used to train the original GRU model is modified, generating an additional 20 000 samples of synthetic data with varying seasonal amplitudes to evaluate the effectiveness of the existing methods. The synthetic data are assumed to consist of three periods, with the amplitude of the seasonality in each period set to differ. Trend and noise components continue to follow previous settings for synthetic simulation data. Table II provides a performance comparison of the proposed VMD-GRU and existing comparative methods on synthetic data with annual seasonal differences.

The results in Table II demonstrate that when an annual difference in the amplitude of the seasonal signal is present, the original GRU model, trained on a fixed amplitude, struggles to handle this change effectively. The performance of the Gaussian filter at different σ levels is significantly impacted by parameter settings, and no specific performance changes correspond to different σ levels. Although the performance of the proposed VMD-GRU model declines relative to the fixed amplitude in Table I, it still significantly outperforms existing methods. An example of the outcomes on the synthetic dataset with annual seasonal variation is visualized in Fig. 11.

The results visualized in Fig. 11 highlight the superior robustness of the proposed VMD-GRU model to annual seasonal variations. Although there are some differences between the seasonal components separated by VMD and the real seasonal components, the annual seasonal variation is fully reflected. Therefore, after the input time series is reconstructed by VMD, the annual seasonal variation is eliminated, and the seasonality in the reconstructed time series can be approximately considered as a constant that does not change with time, which can be easily removed by the GRU in subsequent processing. This robustness renders it more suitable for continuous and large-scale

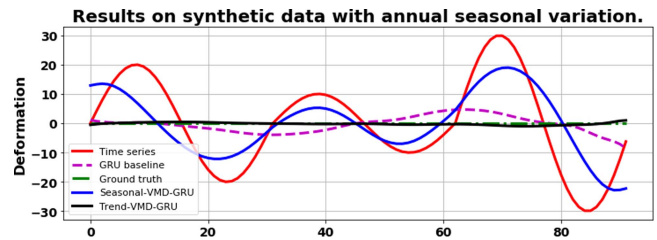


Fig. 11. Example of the results on the synthetic dataset with annual seasonal variation. The original GRU model separates the fixed-amplitude seasonal and trend components shown as blue and purple lines, respectively. Seasonal and trend components separated based on VMD-GRU are shown in green and orange, respectively.

surface deformation monitoring compared to the original GRU model. Interestingly, the original GRU model appears to more frequently align with the smallest amplitude situation in each year, utilizing this as the amplitude for every year. This pattern could potentially explain why the original GRU model assumes a V-shape when an annual-seasonal difference is presented in Fig. 9.

B. Reasons for Time Series Reconstruction

Inspection of Fig. 4(b) and (d) reveals a certain degree of mode mixing between the trend component and the noise component following VMD decomposition. This indicates that direct utilization of VMD decomposition results as the trend component may lead to substantial error. This situation may arise from signal aliasing when VMD is engaged in component decomposition. In the context of InSAR data acquisition, the heterogeneity of atmospheric influence may contribute to outliers, which may originate from sporadic factors influenced by specific meteorological events such as typhoons. These outliers' frequency responses may display low-frequency characteristics similar to the trend signal, thereby leading to a mix of trend components and outliers. While the seasonal component, unlike the trend and noise components, is a signal that manifests around a particular center frequency, as Fig. 4(c) illustrates, i.e., the seasonal component is relatively stable.

Consequently, this study utilizes a data reconstruction method, subtracting the seasonal component decomposed by VMD from the original time series. From a frequency domain perspective, its features are more distinct compared to the trend and noise components. By handling in this way, the influences of outliers and annual seasonal variations originally mixed together are separated. And it is more accurate to separately isolate the seasonal components and use them to reconstruct the input time series data rather than directly employing individual components. This approach leverages the frequency prior introduced by VMD to separate the components and taps into the GRU's exceptional nonlinear feature extraction capabilities. The robustness of the proposed VMD-GRU method is corroborated by the previously presented experimental results on real-world data.

C. Generalization to Different Revisit Periods

The real-world data used thus far to validate the proposed VMD-GRU model were collected in the C-band by Sentinel-1,

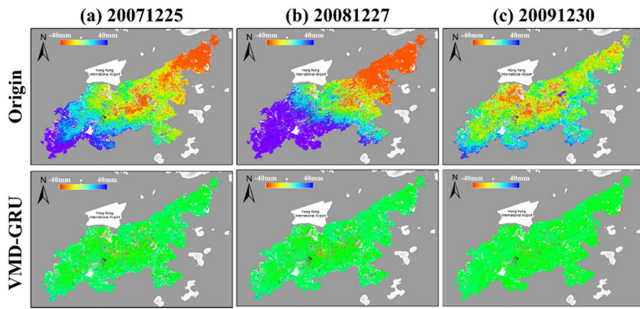


Fig. 12. Performance of VMD-GRU and existing methods on ALOS data.

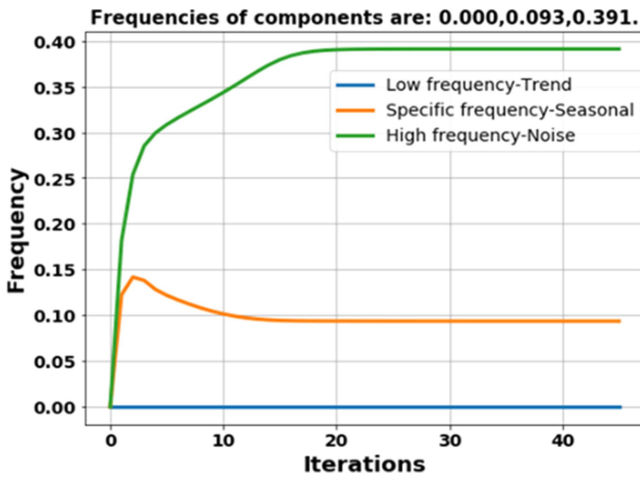


Fig. 13. Spectrum diagram of the ALOS time series data decomposed by VMD.

with a 12-day revisit period. One significant contribution of this study lies in introducing the frequency prior to each component in TS-InSAR to realize timing decomposition from a frequency domain perspective. This naturally raises the question of whether the proposed method can also display strong robustness with different TS-InSAR data that have different revisit periods in various bands.

To address this issue, this study also used the L-band Advanced Land Observing Satellite (ALOS) to obtain the SAR data of Lantau Island from 24 June 2007 to 2 January 2011. The ALOS revisit period is 46 days, unlike the 12-day revisit period of Sentinel-1, which results in a significant shift in the central frequency corresponding to the seasonal components in TS-InSAR. The performance of VMD-GRU and existing methods on ALOS data is shown in Fig. 12.

The periodicity of the ALOS TS-InSAR seasonal component, which has a revisit period of 46 days, is calculated to be $365/46 = 7.9$, with a corresponding central frequency of approximately 0.126. The central frequency associated with the seasonal component shown in Fig. 13 is approximately 0.093, which is in close proximity. These outcomes demonstrate that the proposed VMD-GRU approach is capable of effectively isolating seasonal components from the frequency domain of SAR data collected by satellites with varying revisit periods and across different bands, despite significant changes in center

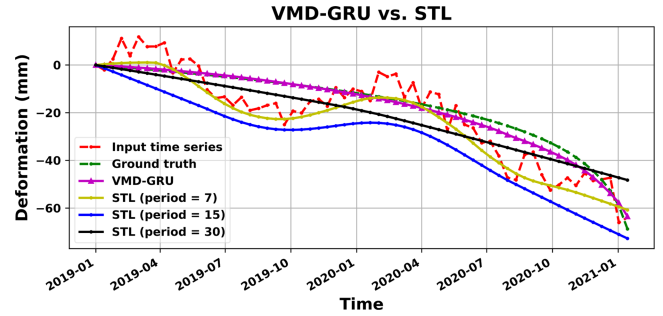


Fig. 14. Comparison between the proposed method and STL with different parameters.

frequency and noise sources. This supplementary experiment on ALOS data further validates the robustness and generalization of the proposed VMD-GRU method. For TS-InSAR data with different revisit periods in different bands, its frequency prior can also be introduced into the VMD-GRU model to improve the robustness and accuracy of continuous large-scale surface deformation monitoring.

For different regions, the seasonal periodic time may be different. The seasonality in some regions can be a year, half a year or both. From the ALOS data experiments, it can be seen that different seasonality will correspond to different center frequencies on the spectrogram. Therefore, the proposed VMD-GRU has better robustness than the fixed periodicity setting method, such as Seasonal-Trend decomposition using LOESS (STL). The comparison between the proposed VMD-GRU method and STL with different parameters is shown in Fig. 14. It can be seen that the existing decoupling methods are easily restricted by parameter selection, while the proposed VMD-GRU shows good generalization.

D. Limitations

While the VMD-GRU model advances the original GRU model by combining VMD and GRU to achieve continuous and large-scale surface deformation monitoring, it only processes the time series data of independent measurement points. It does not incorporate the spatial correlation information of the measurement points into the analysis, which could be significant for understanding local deformation mechanisms and exploring more robust and accurate monitoring. Moreover, there exists a certain degree of aliasing between the trend component and the noise component when using VMD to decompose TS-InSAR into various components. Despite the possibility of further separation by GRU, some remnants may persist. These remnants could be continuously amplified during long-term monitoring, potentially restricting the accuracy of surface deformation trend estimation. In addition, the current approach treats phase unwrapping errors as part of the noise. While this method allows for the effective handling of these errors within the VMD-GRU framework, there is potential for future research to develop specialized techniques for more precise identification and mitigation of phase unwrapping errors, enhancing the overall accuracy and reliability of the monitoring system.

V. CONCLUSION AND FUTURE WORK

This study has made significant efforts to advance the understanding of large-scale surface deformation monitoring through the development and application of the VMD-GRU model. Building on the foundation of the original GRU model, this study proposes a robust surface deformation monitoring method integrating VMD and GRU and explores the introduction of physics-based prior knowledge to the existing deep learning model. This integration has demonstrated superior robustness to outliers and annual seasonal variations, thereby improving continuous and large-scale monitoring potential. Several key conclusions can be drawn from the study.

- 1) The VMD-GRU model is more robust to outlier and annual seasonal variations compared to the original GRU model, demonstrating its applicability in continuous and large-scale surface deformation monitoring.
- 2) The annual seasonal variation, as one of the core factors affecting the accuracy of the existing GRU model, will lead to the accumulation of incompletely separated seasonal components into the trend component, thereby causing errors. This shortcoming can be solved well by introducing the frequency priors of each component in the proposed VMD-GRU model.
- 3) Mode mixing, between the trend component and the noise component, exists after VMD decomposition, suggesting that direct use of VMD decomposition results may cause substantial error. Instead, the VMD-GRU model of reconstructing the input signal and then inputting it into the GRU can effectively improve the robustness of continuous and large-scale surface deformation monitoring.
- 4) The VMD-GRU model proposed in this study has good robustness and generalization and can be well extended to SAR satellites with different revisit periods in different bands when the revisit period is fixed, thus realizing continuous and wide-range ground deformation monitoring across different satellites.

In the future, there are several potential directions worth pursuing. First, the VMD-GRU model could be extended to incorporate spatial correlation information of the measurement points, which could significantly enhance the understanding of local deformation mechanisms and aid in the development of more robust and accurate monitoring methods. This extension would involve analyzing the spatial relationships between PS points and their neighboring points, integrating both temporal and spatial data for more comprehensive deformation analysis. In addition, further exploration is necessary to address the existing aliasing between the trend component and the noise component, which may impact the estimation of surface deformation trends. This research could involve the development of more sophisticated models or techniques to further separate the components and reduce the amplification of remnants during long-term monitoring. By leveraging both frequency-domain decomposition and spatial correlations, the robustness and accuracy of continuous and large-scale surface deformation monitoring can be significantly improved.

APPENDIX A

The pseudocode of the implementation details of VMD is shown in Algorithm 1.

Algorithm 1: Pseudocode for VMD Implementation With Fixed $K = 3$.

- Require:** Signal $s(t)$, Convergence parameter α , Tolerance ϵ
- Ensure:** Modes $u_1(t), u_2(t), u_3(t)$
- 1: Initialize $u_1^{(0)}(t), u_2^{(0)}(t), u_3^{(0)}(t)$, and $\omega_1^{(0)}, \omega_2^{(0)}, \omega_3^{(0)}$
 - 2: Set iteration $n = 0$
 - 3: **repeat:**
 - 4: Solve the following subproblems for $u_1^{(n+1)}, u_2^{(n+1)}, u_3^{(n+1)}$ respectively:

$$u_1^{(n+1)} = \arg \min_{u_1} \mathfrak{R} \left\{ \int \left| \partial_t \left(\left(s(t) - u_2^{(n)}(t) - u_3^{(n)}(t) \right) e^{-i\omega_1^{(n)}t} \right) \right|^2 dt \right\}$$

$$u_2^{(n+1)} = \arg \min_{u_2} \mathfrak{R} \left\{ \int \left| \partial_t \left(\left(s(t) - u_1^{(n+1)}(t) - u_3^{(n)}(t) \right) e^{-i\omega_2^{(n)}t} \right) \right|^2 dt \right\}$$

$$u_3^{(n+1)} = \arg \min_{u_3} \mathfrak{R} \left\{ \int \left| \partial_t \left(\left(s(t) - u_1^{(n+1)}(t) - u_2^{(n+1)}(t) \right) e^{-i\omega_3^{(n)}t} \right) \right|^2 dt \right\}.$$
 - 5: Compute the new center frequencies by taking the first moment of the spectrum for each mode:

$$\omega_1^{(n+1)} = \frac{\int \omega \left| \hat{u}_1^{(n+1)}(\omega) \right|^2 d\omega}{\int \left| \hat{u}_1^{(n+1)}(\omega) \right|^2 d\omega}$$

$$\omega_2^{(n+1)} = \frac{\int \omega \left| \hat{u}_2^{(n+1)}(\omega) \right|^2 d\omega}{\int \left| \hat{u}_2^{(n+1)}(\omega) \right|^2 d\omega}$$

$$\omega_3^{(n+1)} = \frac{\int \omega \left| \hat{u}_3^{(n+1)}(\omega) \right|^2 d\omega}{\int \left| \hat{u}_3^{(n+1)}(\omega) \right|^2 d\omega}$$

- 6: Set $n = n + 1$
 - 7: **Until** convergence criteria is met,
 $\max |\omega_k^{(n)} - \omega_k^{(n-1)}| < \text{for all } k$
-

APPENDIX B

GRU is a type of RNN that has proven effective in processing sequential data. However, they face challenges when dealing with missing or irregularly sampled data. To address these issues, the GRU-D model was proposed, which incorporates additional information about missing data and time intervals between observations.

B.1 Gated Recurrent Units

GRU is a simplified variant of LSTM units, another type of RNN. The GRU model uses gating units to modulate the flow of information, but unlike the LSTM, it does not have a separate memory cell and uses fewer gates, making it computationally more efficient.

The updated equations for a GRU are as follows:

$$\begin{aligned} r_t &= \sigma(W_r x_t + U_r h_{t-1} + b_r) \\ z_t &= \sigma(W_z x_t + U_z h_{t-1} + b_z) \\ \tilde{h}_t &= \tanh(W x_t + U(r_t \odot h_{t-1}) + b) \\ h_t &= (1 - z_t) \odot h_{t-1} + z_t \odot \tilde{h}_t \end{aligned} \quad (10)$$

where x_t is the input at time t , h_{t-1} is the hidden state at the previous time step, σ is the sigmoid function, \odot denotes element-wise multiplication, and W , U , and b are learnable parameters.

B.2 GRU With Decay

GRU-D extends the GRU model to handle missing values and irregular time intervals in time-series data. It introduces additional inputs: a masking vector to indicate missing values and a time interval vector to capture the time elapsed since the last observation.

The update equations for a GRU-D are similar to those of a GRU, but with additional transformations to handle missing data and irregular time intervals

$$\begin{aligned} r_t &= \sigma(W_r \hat{x}_t + U_r \hat{h}_{t-1} + V_r m_t + b_r) \\ z_t &= \sigma(W_z \hat{x}_t + U_z \hat{h}_{t-1} + V_z m_t + b_z) \\ \tilde{h}_t &= \tanh(W \hat{x}_t + U(r_t \odot \hat{h}_{t-1}) + V m_t + b) \\ h_t &= (1 - z_t) \odot \hat{h}_{t-1} + z_t \odot \tilde{h}_t \end{aligned} \quad (11)$$

where m_t is the masking vector at time t , indicating the presence of missing values, and V is the time interval vector at time t , representing the time elapsed since the last observation.

REFERENCES

- [1] D. Festa et al., "Nation-wide mapping and classification of ground deformation phenomena through the spatial clustering of p-SBAS InSAR measurements: Italy case study," *ISPRS J. Photogrammetry Remote Sens.*, vol. 189, pp. 1–22, 2022, doi: [10.1016/j.isprsjprs.2022.04.022](https://doi.org/10.1016/j.isprsjprs.2022.04.022).
- [2] Z. Lu, O. Kwoun, and R. Rykhus, "Interferometric synthetic aperture radar (InSAR): Its past, present and future," *Photogrammetric Eng. Remote Sens.*, vol. 73, no. 3, p. 217, 2007, doi: [10.1016/j.isprsjprs.2022.04.022](https://doi.org/10.1016/j.isprsjprs.2022.04.022).
- [3] Z. Ma et al., "Towards big SAR data era: An efficient Sentinel-1 near-real-time InSAR processing workflow with an emphasis on co-registration and phase unwrapping," *ISPRS J. Photogrammetry Remote Sens.*, vol. 188, pp. 286–300, 2022, doi: [10.1016/j.isprsjprs.2022.04.013](https://doi.org/10.1016/j.isprsjprs.2022.04.013).
- [4] B. Yu et al., "Coal fire identification and state assessment by integrating multitemporal thermal infrared and InSAR remote sensing data: A case study of Midong district, Urumqi, China," *ISPRS J. Photogrammetry Remote Sens.*, vol. 190, pp. 144–164, 2022, doi: [10.1016/j.isprsjprs.2022.06.007](https://doi.org/10.1016/j.isprsjprs.2022.06.007).
- [5] Z. Zhang, Q. Zeng, and J. Jiao, "Deformations monitoring in complicated-surface areas by adaptive distributed scatterer InSAR combined with land cover: Taking the Jiaju landslide in Danba, China as an example," *ISPRS J. Photogrammetry Remote Sens.*, vol. 186, pp. 102–122, 2022, doi: [10.1016/j.isprsjprs.2022.02.004](https://doi.org/10.1016/j.isprsjprs.2022.02.004).
- [6] A. Ferretti, C. Prati, and F. Rocca, "Permanent scatterers in SAR interferometry," *IEEE Trans. Geosci. Remote Sens.*, vol. 39, no. 1, pp. 8–20, Jan. 2001, doi: [10.1109/36.898661](https://doi.org/10.1109/36.898661).
- [7] B. Osmanoglu, F. Sunar, S. Wdowinski, and E. Cabral-Cano, "Time series analysis of InSAR data: Methods and trends," *ISPRS J. Photogrammetry Remote Sens.*, vol. 115, pp. 90–102, 2016, doi: [10.1016/j.isprsjprs.2015.10.003](https://doi.org/10.1016/j.isprsjprs.2015.10.003).
- [8] Q. Zhao et al., "Generation of long-term InSAR ground displacement time-series through a novel multi-sensor data merging technique: The case study of the Shanghai coastal area," *ISPRS J. Photogrammetry Remote Sens.*, vol. 154, pp. 10–27, 2019, doi: [10.1016/j.isprsjprs.2019.05.005](https://doi.org/10.1016/j.isprsjprs.2019.05.005).
- [9] P. K. Kirui, E. Reinosch, N. Isya, B. Riedel, and M. Gerke, "Mitigation of atmospheric artefacts in multi temporal InSAR: A review," *PFG–J. Photogrammetry, Remote Sens. Geoinformation Sci.*, vol. 89, pp. 251–272, 2021, doi: [10.1007/s41064-021-00138-z](https://doi.org/10.1007/s41064-021-00138-z).
- [10] P. K. Kirui, B. Riedel, and M. Gerke, "Multi-temporal InSAR tropospheric delay modelling using Tikhonov regularization for Sentinel-1 c-band data," *ISPRS Open J. Photogrammetry Remote Sens.*, vol. 6, 2022, Art. no. 100020, doi: [100020](https://doi.org/10.1016/j.ophoto.2022.100020). [10.1016/j.ophoto.2022.100020](https://doi.org/10.1016/j.ophoto.2022.100020).
- [11] M. Schlögl, B. Widhalm, and M. Avian, "Comprehensive time-series analysis of bridge deformation using differential satellite radar interferometry based on Sentinel-1," *ISPRS J. Photogrammetry Remote Sens.*, vol. 172, pp. 132–146, 2021, doi: [10.1016/j.isprsjprs.2020.12.001](https://doi.org/10.1016/j.isprsjprs.2020.12.001).
- [12] F. Hu et al., "Error analysis and 3D reconstruction using airborne array InSAR images," *ISPRS J. Photogrammetry Remote Sens.*, vol. 190, pp. 113–128, 2022, doi: [10.1016/j.isprsjprs.2022.06.005](https://doi.org/10.1016/j.isprsjprs.2022.06.005).
- [13] P. Ma et al., "Remotely sensing large-and small-scale ground subsidence: A case study of the Guangdong–Hong Kong–Macao greater bay area of China," *Remote Sens. Environ.*, vol. 232, 2019, Art. no. 111282, doi: [10.1016/j.rse.2019.111282](https://doi.org/10.1016/j.rse.2019.111282).
- [14] R. F. Hanssen, *Radar Interferometry: Data interpretation and Error Analysis*, vol. 2. New York, NY, USA: Springer-Verlag, 2001, doi: [10.1007/0-306-47633-9](https://doi.org/10.1007/0-306-47633-9).
- [15] D. Bekaert, R. Walters, T. Wright, A. Hooper, and D. Parker, "Statistical comparison of InSAR tropospheric correction techniques," *Remote Sens. Environ.*, vol. 170, pp. 40–47, 2015, doi: [10.1016/j.rse.2015.08.035](https://doi.org/10.1016/j.rse.2015.08.035).
- [16] H. Fattahi and F. Amelung, "InSAR bias and uncertainty due to the systematic and stochastic tropospheric delay," *J. Geophysical Res., Solid Earth*, vol. 120, no. 12, pp. 8758–8773, 2015, doi: [10.1002/2015JB012419](https://doi.org/10.1002/2015JB012419).
- [17] C. Yu, N. T. Penna, and Z. Li, "Generation of real-time mode high-resolution water vapor fields from GPS observations," *J. Geophysical Res., Atmos.*, vol. 122, no. 3, pp. 2008–2025, 2017, doi: [10.1002/2016JD025753](https://doi.org/10.1002/2016JD025753).
- [18] Z. Li et al., "Time-series InSAR ground deformation monitoring: Atmospheric delay modeling and estimating," *Earth-Sci. Rev.*, vol. 192, pp. 258–284, 2019, doi: [10.1016/j.earscirev.2019.03.008](https://doi.org/10.1016/j.earscirev.2019.03.008).
- [19] W. Mao et al., "Ionospheric phase delay correction for time series multi-aperture InSAR constrained by polynomial deformation model," *IEEE Geosci. Remote Sens. Lett.*, vol. 20, 2023, Art. no. 4006605, doi: [10.1109/LGRS.2023.3281343](https://doi.org/10.1109/LGRS.2023.3281343).
- [20] A. Ferretti, C. Prati, and F. Rocca, "Nonlinear subsidence rate estimation using permanent scatterers in differential SAR interferometry," *IEEE Trans. Geosci. Remote Sens.*, vol. 38, no. 5, pp. 2202–2212, Sep. 2000, doi: [10.1109/36.868878](https://doi.org/10.1109/36.868878).
- [21] P. Ma et al., "Remotely sensing large-and small-scale ground subsidence: A case study of the Guangdong–Hong Kong–Macao greater bay area of China," *Remote Sens. Environ.*, vol. 232, 2019, Art. no. 111282, doi: [10.1016/j.rse.2019.111282](https://doi.org/10.1016/j.rse.2019.111282).
- [22] P. Ma, F. Zhang, and H. Lin, "Prediction of InSAR time-series deformation using deep convolutional neural networks," *Remote Sens. Lett.*, vol. 11, no. 2, pp. 137–145, 2020, doi: [10.1080/2150704X.2019.1692390](https://doi.org/10.1080/2150704X.2019.1692390).
- [23] Z. Jiao, G. Jia, and Y. Cai, "A new approach to oil spill detection that combines deep learning with unmanned aerial vehicles," *Comput. Ind. Eng.*, vol. 135, pp. 1300–1311, 2019, doi: [10.1016/j.cie.2018.11.008](https://doi.org/10.1016/j.cie.2018.11.008).
- [24] D. Amodei et al., "Deep speech 2: End-to-end speech recognition in English and Mandarin," in *Proc. Int. Conf. Mach. Learn.*, 2016, pp. 173–182.
- [25] A. Vaswani et al., "Attention is all you need," *Adv. Neural Inf. Process. Syst.*, vol. 30, pp. 6000–6010, 2017.
- [26] S. Hochreiter and J. Schmidhuber, "Long short-term memory," *Neural Computation*, vol. 9, no. 8, pp. 1735–1780, 1997, doi: [10.1162/neco.1997.9.8.1735](https://doi.org/10.1162/neco.1997.9.8.1735).
- [27] K. Cho et al., "Learning phrase representations using RNN encoder-decoder for statistical machine translation," 2014, *arXiv:1406.1078*.
- [28] Y. Cai et al., "A high-performance and in-season classification system of field-level crop types using time-series landsat data and a machine learning approach," *Remote Sens. Environ.*, vol. 210, pp. 35–47, 2018, doi: [10.1016/j.rse.2018.02.045](https://doi.org/10.1016/j.rse.2018.02.045).

[29] D. Ienco, R. Gaetano, C. Dupaquier, and P. Maurel, "Land cover classification via multitemporal spatial data by deep recurrent neural networks," *IEEE Geosci. Remote Sens. Lett.*, vol. 14, no. 10, pp. 1685–1689, Oct. 2017, doi: [10.1109/LGRS.2017.2728698](https://doi.org/10.1109/LGRS.2017.2728698).

[30] P. Ma et al., "Improving time-series InSAR deformation estimation for city clusters by deep learning-based atmospheric delay correction," *Remote Sens. Environ.*, vol. 304, 2024, Art. no. 114004, doi: [10.1016/j.rse.2024.114004](https://doi.org/10.1016/j.rse.2024.114004).

[31] E. Intriери et al., "The Maoxian landslide as seen from space: Detecting precursors of failure with Sentinel-1 data," *Landslides*, vol. 15, pp. 123–133, 2018, doi: [10.1007/s10346-017-0915-7](https://doi.org/10.1007/s10346-017-0915-7).

[32] Z. Zhao, Z. Wu, Y. Zheng, and P. Ma, "Recurrent neural networks for atmospheric noise removal from InSAR time series with missing values," *ISPRS J. Photogrammetry Remote Sens.*, vol. 180, pp. 227–237, 2021, doi: [10.1016/j.isprsjprs.2021.08.009](https://doi.org/10.1016/j.isprsjprs.2021.08.009).

[33] A. Shakeel, R. J. Walters, S. K. Ebmeier, and N. A. Moubayed, "ALADDIn: Autoencoder-LSTM-based anomaly detector of deformation in InSAR," *IEEE Trans. Geosci. Remote Sens.*, vol. 60, 2022, Art. no. 4706512, doi: [10.1109/TGRS.2022.3169455](https://doi.org/10.1109/TGRS.2022.3169455).

[34] J. Du, K. Yin, and S. Lacasse, "Displacement prediction in colluvial landslides, three Gorges reservoir, China," *Landslides*, vol. 10, pp. 203–218, 2013, doi: [10.1007/s10346-012-0326-8](https://doi.org/10.1007/s10346-012-0326-8).

[35] C. Zhou, K. Yin, Y. Cao, and B. Ahmed, "Application of time series analysis and PSO-SVM model in predicting the Bazimen landslide in the three gorges reservoir, China," *Eng. Geol.*, vol. 204, pp. 108–120, 2016, doi: [10.1016/j.engeo.2016.02.009](https://doi.org/10.1016/j.engeo.2016.02.009).

[36] P. Ma et al., "Toward fine surveillance: A review of multitemporal interferometric synthetic aperture radar for infrastructure health monitoring," *IEEE Geosci. Remote Sens. Mag.*, vol. 10, no. 1, pp. 207–230, Mar. 2022, doi: [10.1109/MGRS.2021.3098182](https://doi.org/10.1109/MGRS.2021.3098182).

[37] D. Sandwell, R. Mellors, X. Tong, M. Wei, and P. Wessel, *Open Radar Interferometry Software for Mapping Surface Deformation*. Hoboken, NJ, USA: Wiley, 2011, doi: [10.1029/2011EO280002](https://doi.org/10.1029/2011EO280002).

[38] A. Ferretti, A. Fumagalli, F. Novali, C. Prati, F. Rocca, and A. Rucci, "A new algorithm for processing interferometric data-stacks: SqueeSAR," *IEEE Trans. Geosci. Remote Sens.*, vol. 49, no. 9, pp. 3460–3470, Sep. 2011, doi: [10.1109/TGRS.2011.2124465](https://doi.org/10.1109/TGRS.2011.2124465).

[39] K. Dragomiretskiy and D. Zosso, "Variational mode decomposition," *IEEE Trans. Signal Process.*, vol. 62, no. 3, pp. 531–544, Feb. 2014, doi: [10.1109/TSP.2013.2288675](https://doi.org/10.1109/TSP.2013.2288675).

[40] N. E. Huang et al., "The empirical mode decomposition and the Hilbert spectrum for nonlinear and non-stationary time series analysis," *Proc. Roy. Soc. London Ser. A, Math., Phys. Eng. Sci.*, vol. 454, no. 1971, pp. 903–995, 1998, doi: [10.1098/rspa.1998.0193](https://doi.org/10.1098/rspa.1998.0193).

[41] P. S. Addison, *The Illustrated Wavelet Transform Handbook: Introductory Theory and Applications in Science, Engineering, Medicine and Finance*. Boca Raton, FL, USA: CRC Press, 2017, doi: [10.1887/0750306920](https://doi.org/10.1887/0750306920).

[42] C. Kaur, A. Bisht, P. Singh, and G. Joshi, "EEG signal denoising using hybrid approach of variational mode decomposition and wavelets for depression," *Biomed. Signal Process. Control*, vol. 65, 2021, Art. no. 102337, doi: [10.1016/j.bspc.2020.102337](https://doi.org/10.1016/j.bspc.2020.102337).

[43] B. Pang, M. Nazari, and G. Tang, "Recursive variational mode extraction and its application in rolling bearing fault diagnosis," *Mech. Syst. Signal Process.*, vol. 165, 2022, Art. no. 108321, doi: [10.1016/j.ymsp.2021.108321](https://doi.org/10.1016/j.ymsp.2021.108321).

[44] C. Li and M. Liang, "Time-frequency signal analysis for gearbox fault diagnosis using a generalized synchrosqueezing transform," *Mech. Syst. Signal Process.*, vol. 26, pp. 205–217, 2012, doi: [10.1016/j.ymsp.2011.07.001](https://doi.org/10.1016/j.ymsp.2011.07.001).

[45] D. Hilbert, *Grundzuge Einer Allgemeinen Theorie Der Linearen Integralgleichungen*. New York, NY, USA: Chelsea, 1953, pp. 1–282.

[46] D. P. Bertsekas, "Multiplier methods: A survey," *Automatica*, vol. 12, no. 2, pp. 133–145, 1976, doi: [10.1016/0005-1098\(76\)90077-7](https://doi.org/10.1016/0005-1098(76)90077-7).

[47] J. Nocedal and S. J. Wright, *Numerical Optimization*. Berlin, Germany: Springer-Verlag, 1999.

[48] D. Bertsekas, *Lagrange Multiplier Methods in Constrained Optimization*. New York, NY, USA: Academic, 1982.

[49] M. R. Hestenes, "Multiplier and gradient methods," *J. Optim. Theory Appl.*, vol. 4, no. 5, pp. 303–320, 1969, doi: [10.1007/BF00927673](https://doi.org/10.1007/BF00927673).

[50] R. T. Rockafellar, "A dual approach to solving nonlinear programming problems by unconstrained optimization," *Math. Program.*, vol. 5, no. 1, pp. 354–373, 1973, doi: [10.1007/BF01580138](https://doi.org/10.1007/BF01580138).

[51] M. Nazari and S. M. Sakhaei, "Variational mode extraction: A new efficient method to derive respiratory signals from ECG," *IEEE J. Biomed. Health Informat.*, vol. 22, no. 4, pp. 1059–1067, Jul. 2018, doi: [10.1109/JBHI.2017.2734074](https://doi.org/10.1109/JBHI.2017.2734074).

[52] Z. Che, S. Purushotham, K. Cho, D. Sontag, and Y. Liu, "Recurrent neural networks for multivariate time series with missing values," *Sci. Rep.*, vol. 8, no. 1, 2018, Art. no. 6085, doi: [10.1038/s41598-018-24271-9](https://doi.org/10.1038/s41598-018-24271-9).

[53] D. Bahdanau, K. Cho, and Y. Bengio, "Neural machine translation by jointly learning to align and translate," 2014, *arXiv:1409.0473*.

[54] M. Abadi et al., "TensorFlow: Large-scale machine learning on heterogeneous systems," 2015. [Online]. Available: <https://www.tensorflow.org/>

[55] D. P. Kingma and J. Ba, "Adam: A method for stochastic optimization," 2014, *arXiv:1412.6980*.

[56] G. Blewitt, W. C. Hammond, and C. Kreemer, "Harnessing the GPS data explosion for interdisciplinary science," *Eos*, 99, 2018.

[57] J. Ding, J. Chen, J. Wang, and Y. Zhang, "Characteristic differences in tropospheric delay between nevada geodetic laboratory products and NWM ray-tracing," *GPS Solutions*, vol. 27, no. 1, pp. 1–12, 2023, doi: [10.1007/s10291-022-01385-2](https://doi.org/10.1007/s10291-022-01385-2).

[58] C. Colesanti, A. Ferretti, F. Novali, C. Prati, and F. Rocca, "SAR monitoring of progressive and seasonal ground deformation using the permanent scatterers technique," *IEEE Trans. Geosci. Remote Sens.*, vol. 41, no. 7, pp. 1685–1701, Jul. 2003.



Peifeng Ma (Senior Member, IEEE) received the M.S. degree in signal and information processing from the Institute of Remote Sensing and Digital Earth, Chinese Academy of Sciences, Beijing, China, in 2012, and the Ph.D. degree in Earth system and geoinformation science from the Institute of Space and Earth Information Science, The Chinese University of Hong Kong, Hong Kong, in 2016.

He is currently an Assistant Professor with the Department of Geography and Resource Management, Institute of Space and Earth Information Science,

The Chinese University of Hong Kong. He has authored or coauthored more than 50 research articles in high-impact peer-reviewed journals, such as the *Remote Sensing of Environment*, *IEEE TRANSACTIONS ON GEOSCIENCE AND REMOTE SENSING*, and the *International Society for Photogrammetry and Remote Sensing (ISPRS) Journal of Photogrammetry and Remote Sensing*. He is the Principal Coordinator of the Development of an intelligent infrastructural health diagnosis-oriented interferometric synthetic aperture radar platform project in Hong Kong. His research interests include persistent scatterer interferometry, synthetic aperture radar tomography, distributed scatterer interferometry, and their applications for urban infrastructural health monitoring and geo-hazard monitoring.



Zeyu Jiao received the B.Eng. degree in aerospace propulsion engineering and the Ph.D. degree in information management from Beihang University, Beijing, China, in 2015 and 2020, respectively.

He is currently a Postdoctoral Fellow with the Institute of Space and Earth Information Science (ISEIS), the Chinese University of Hong Kong, Hong Kong. His recent studies focus on exploring and extracting spatiotemporal features for long-term and large-scale surface deformation monitoring. His research interests include machine/deep learning, and InSAR time-

series analysis.



Zherong Wu (Member, IEEE) received the B.Eng. degree in remote sensing from Wuhan University, Wuhan, China, in 2019, and the Ph.D. degree in Earth system and geoinformation science from the Institute of Space and Earth Information Science, Chinese University of Hong Kong, Hong Kong, in 2023.

She is currently a Postdoctoral Associate with the College of Agriculture and Life Sciences, Cornell University, Ithaca, NY, USA, working with Prof. Ying Sun, where her research focuses on integrating mul-

ti-source satellite remote sensing, land surface modeling, and deep learning to advance carbon neutrality and sustainable development. Her Ph.D. degree was supervised by Prof. Peifeng Ma, Prof. Hongsheng Li and Prof. Mei-Po Kwan. In addition, in 2022, she served as a Research Intern with the United Nations Economic and Social Commission for Asia and the Pacific.